ACS APPLIED MATERIALS & INTERFACES

Research Article

www.acsami.org

Ferritin-Templated Synthesis and Self-Assembly of Pt Nanoparticles on a Monolithic Porous Graphene Network for Electrocatalysis in Fuel Cells

Huajun Qiu,[†,∥,⊥] Xiaochen Dong,[‡,∥] Barindra Sana,[†] Tao Peng,[†] David Paramelle,[§] Peng Chen,[†] and Sierin Lim*[,†]

[†]Division of Bioengineering, School of Chemical and Biomedical Engineering, Nanyang Technological University, 70 Nanyang Drive, Block N1.3, Singapore 637457

[‡]Institute of Advanced Materials (IAM), Nanjing University of Technology, 210009, China

[§]Institute of Materials Research and Engineering, Agency for Science, Technology and Research (A*STAR), 3 Research Link, Singapore 117602

Supporting Information

ABSTRACT: The monolithic three-dimensional (3D) graphene network is used as the support for Pt nanoparticles (NPs) to fabricate an advanced 3D graphene-based electrocatalyst. Distinct from previous strategies, the monodispersed Pt NPs with ultrafine particle size (~3 nm) are synthesized using ferritin protein nanocages as the template and subsequently self-assembled on the 3D graphene by leveraging on the hydrophobic interaction between the ferritin and the graphene. Following the self-assembly, the ferritins are removed, resulting in a stable Pt NP/3D graphene composite. The composite exhibits much enhanced electrocatalytic activity for methanol oxidation as compared with both Pt NP/chemically reduced graphene oxide (Pt/r-GO) and state-of-the-art Pt/C catalyst. The observed electrocatalytic activity also shows marked improvement over Pt/3D graphene prepared by pulse electrodeposition of Pt. This study demonstrates that protein nanocage templating and assembly are promising strategies for the fabrication of functional composites in catalysis and fuel cell applications.

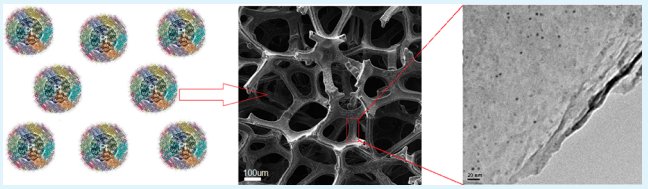

KEYWORDS: *three-dimensional graphene, ferritin, protein nanocage, Pt electrocatalyst, fuel cells*

INTRODUCTION

Graphene, a two-dimensional single-layer sheet of graphite with fully delocalized p-electrons on the graphitic plane, has unique physicochemical properties, such as high surface area, high conductivity, and mechanical strength.[1−12] The unique physicochemical properties make graphene attractive as a material for molecular electronic devices, energy storage, and catalytic applications.[13−18] In catalytic studies, graphene powder (i.e., reduced graphene oxide, r-GO) has been traditionally used as a catalyst/electrocatalyst support because of the low-cost and large-scale production enabled by the chemical exfoliation processes.[3,4,6,7] The use of r-GO has been reported to impair the unique graphene properties due to the abundant defects and functional moieties created during the synthesis procedures.[19] The aggregation and stacking between individual graphene sheets driven by strong $\pi-\pi$ interaction result not only in significant reduction in active surface area but also in compromised conductivity.

Compared with reduced graphene powder, the monolithic three-dimensional (3D) graphene architecture (recently demonstrated by the chemical vapor deposition (CVD) method[20]) is expected to exhibit enhanced property for certain applications. For example, when used as an electrocatalyst support, the close contact between electrocatalysts and graphene plays an important role in the catalyst activity enhancement. Growing Pt (or Pd)-based nanoparticle (NP) catalysts directly on the graphene surface maximizes graphene−NP contact and results in the desired high catalytic activity.[4,6] The NPs prepared from the in situ growth method usually lack the desired size and morphology controls, and their catalytic potentials may not be fully realized. With the recent progress in solution-phase synthesis of uniform and monodispersed NPs, the assembly of these NPs on the graphene surface may be expected to be a better approach to prepare the NP/graphene composite for NP activity optimization.[3,21] However, the synthesis and deposition of ultrafine metal NPs on the graphene surface has been relatively challenging due to the aggregation tendency of these ultrafine NPs and the hydrophobic nature of graphene.

Biological molecules have been proposed as a nanoreactor for the synthesis of monodispersed ultrafine NPs,[22] while their rich surface properties facilitate further modification and

Received: October 16, 2012
Accepted: January 2, 2013
Published: January 18, 2013

immobilization.[23] Ferritins are important iron storage molecules found in most living systems. The self-assembly of 24 identical subunits form a roughly spherical hollow ferritin nanocage with an external diameter of ~12 nm and a cavity diameter of ~8 nm.[24] The channels formed between the subunits allow the transport of metal ions into and out of the cavity. Physiologically, ferritins convert soluble ferrous salts into a ferric complex which is then stored within the cavity. In *in vitro* experiment, each cavity can be loaded with up to 7000 iron atoms, forming a nanoparticle with a protein shell.[25] *In vitro* metal nanoparticle synthesis within the cavity of ferritins is not limited to iron. Recently, ferritins have also been successfully used for the syntheses of various protein–inorganic hybrids, such as Pt, Pd, Au, Ag, FeS, CdS, CeSe, and ZnSe cores with ferritin shells.[22,26,27] The ferritin-templated synthesis of nanoparticles offers high precision size control and monodispersity. These biocomposites have been shown to be promising in various applications such as catalysis, drug delivery, sensing, and magnetic resonance imaging (MRI). For example, MnOOH and FeOOH core–ferritin shell biocomposites have been successfully prepared as a potential contrast agent in MRI in our previous work.[25,28] In this work, using ferritin (Ftn) as a template and nanoreactor, we synthesize Pt NP–core with ferritin–shell ((Pt)Ftn) biocomposites, which are then self-assembled on the surface of a monolithic 3D graphene network to fabricate a unique nanocomposite material. After the removal of the protein shell, the Pt NPs' (~3 nm) decorated porous graphene network shows excellent performance as an electrocatalyst for methanol oxidation reaction (MOR) and is promising as an anode catalyst in direct methanol fuel cells (DMFCs).

EXPERIMENTAL SECTION

Synthesis of 3D Graphene Foams. The 3D graphene was fabricated by chemical vapor deposition (CVD) using Ni foam as the substrate and ethanol as the carbon source.[20,29,30] The 0.5 mm thickness Ni foam (Alantum Advanced Technology Materials) was placed into a quartz tube and heated to 1000 °C at a rate of 50 °C min^{-1}. Under this condition, the Ni foam surface was cleaned by flowing H_2/Ar (H_2:Ar = 25:50 sccm) gas for 10 min under atmospheric pressure. Subsequently, ethanol was introduced into the tube for graphene growth for 20 min. The resulting product was quickly cooled to room temperature at a cooling rate of 100 °C min^{-1} under the H_2/Ar flow. The sample was eventually cut into uniform pieces (1 cm × 1 cm), and the Ni substrate was removed by etching in 3 M HCl aqueous solution to obtain the free-standing 3D graphene foam.

Preparation of (Pt)Ftn and Pt NP/Graphene Composite. Cloning, expression, and purification of the engineered *Archaeoglobus fulgidus* ferritin (Ftn) were carried out following a previously described method.[25,31] The unloaded Ftn (apo-Ftn) was quantified by the bicinchoninic acid (BCA) method. K_2PtCl_4 (24 mM) was added dropwise into apo-Ftn solution (1 mM, pH 8.5) until a theoretical loading of 20 metal atoms per ferritin was achieved. The mixture was stirred for 2 h at room temperature. Subsequently, a solution of $NaBH_4$ (10 mM) was added to the mixture and stirred for an additional 3 h at room temperature.

The monolithic Pt NP/3D graphene composite was prepared by first incubating the 3D graphene (1 cm × 1 cm) in a (Pt)Ftn solution (5 mL, 1.0 mM) for 10 h. The thoroughly rinsed (Pt)Ftn/3D graphene composite was subsequently heated to 400 °C at a rate of 5 °C/min in a nitrogen atmosphere to remove the protein shell.[32] GO was prepared using natural graphite powder through a modified Hummers method[33] and reduced by N_2H_4 to form black r-GO precipitate. The r-GO (3 mg) was mixed with (Pt)Ftn (5 mL, 1.0 mM) for 10 h. The product was then centrifuged and heated to 400 °C to obtain the Pt/r-GO. Commercial Pt/C (20 wt % on carbon) was obtained from Johnson-Matthey Company. The Pt/3D graphene was used as a free-standing electrode. The Pt/r-GO and Pt/C were deposited on a glassy carbon electrode (4 mm in diameter) surface with the help of 0.05 wt % Nafion.

Characterization. The formation of (Pt)Ftn core–shell structures was monitored by the change of hydrodynamic diameter using a Zetasizer Nano ZS dynamic light scattering (DLS) instrument (Malvern Instruments) at 25 °C. To determine the amount of Pt in ferritin, the (Pt)Ftn was dissolved in a fresh mixture of concentrated nitric acid and hydrochloric acid (volumetric ratio of 1:3) to form chloroplatinic acid, and the Pt content was determined by inductively coupled plasma atomic emission spectroscopy (ICP-AES). The morphologies of all samples were characterized using either a JSM-6700F field-emission scanning electron microscope (SEM), a JEM-1400 transmission electron microscope (TEM), or a Philips CM300 high-resolution TEM (HRTEM). X-ray diffraction (XRD) analysis was performed on an advanced X-ray diffractometer (Bruker D8, Cu Kα radiation, and step rate: 0.04° s^{-1}). The Raman spectra (excited at 488 nm) were obtained on a confocal Raman microscope (CRM200, WITec). Electrochemical tests were carried out on a CHI660C potentiostat (CH Instrument Company) using a standard three-electrode cell with a monolithic 3D graphene composite, a Pt foil, and a saturated calomel electrode (SCE) as working, counter, and reference electrodes, respectively. All the potentials given in this paper were vs SCE.

RESULTS AND DISCUSSION

Material Preparation and Characterization. The as-prepared 3D graphene foam is monolithic with good mechanical stability and is easily handled (Figure 1a).

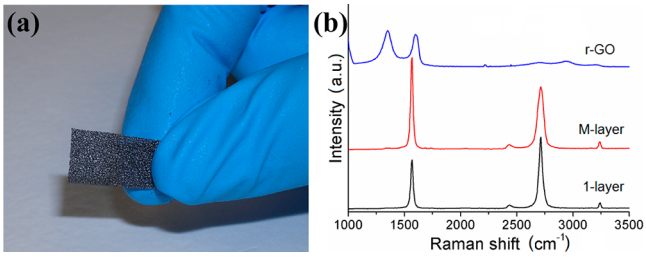

Figure 1. Photograph of the as-prepared monolithic 3D graphene foam (a) and Raman spectra of r-GO and 3D graphene measured at different spots (b).

Characterization of the monolithic graphene by Raman spectroscopy (Figure 1b) reveals two characteristic peaks at ~1560 cm^{-1} (G band) and ~2700 cm^{-1} (2D band) which are consistent with previously published results.[34] It is known that the intensity of the G band (I_G) increases monotonically with the increase of graphene thickness, whereas I_{2D} is relatively stable and I_G/I_{2D} scales linearly with the number of graphene layers (up to 4 layers).[35] The integrated intensity ratio of G and 2D bands (I_G/I_{2D}) in the Raman spectrum obtained at different spots indicates that the 3D graphene contains both single-layer and few-layer domains (Figure 1b).[36] The Raman D band (at ~1350 cm^{-1}) is originated from the disordered carbon in graphene, and its intensity indicates the density of defects in the as-grown graphene film.[37] The extremely weak D band in the Raman spectra (Figure 1b) suggests that the obtained monolithic 3D graphene is of high quality. The D/G intensity ratio of the r-GO indicates that the GO has been reduced to graphene. A similar D/G intensity ratio has also been observed from reduced GO in previous work.[4] Figure 2a and b shows low-magnification SEM images of the Ni foam substrate and

dx.doi.org/10.1021/am3022366 | ACS Appl. Mater. Interfaces 2013, 5, 782–787

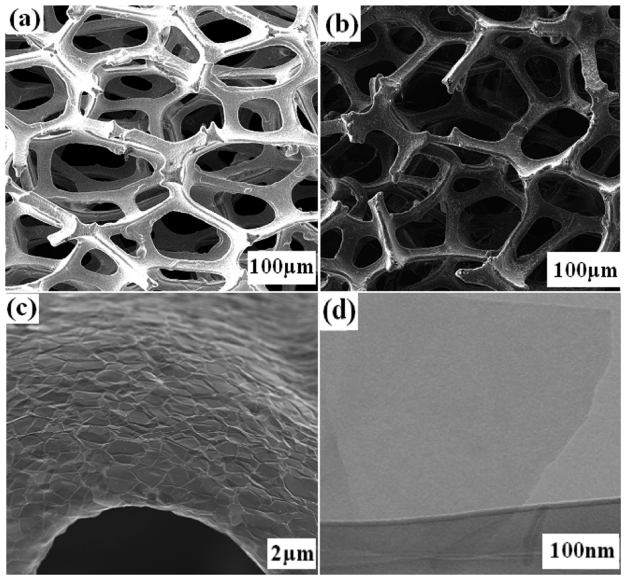

Figure 2. SEM images of Ni foam (a) and 3D graphene (b and c); TEM image of the 3D graphene after a mild ultrasonic treatment (d).

the monolithic 3D graphene, respectively. The pore-ligament morphology of the Ni foam is well-inherited by the monolithic graphene as shown by the open pores of hundreds of micrometers and the graphene network with a diameter of ~100 μm. Figure 2c shows the high-magnification SEM image of the 3D graphene surface which exhibits a scale-like morphology. The TEM image of the ultrasonic-treated 3D graphene in Figure 2d further demonstrates the graphene monolayer nature of most connected ligaments. Energy-dispersive X-ray spectroscopy (EDX) analysis shows that some Ni residue remains after Ni foam etching.[13]

Controlling the size and dispersion of Pt NPs on 3D graphene is critical for electrocatalysis application. The synthesis of monodispersed Pt NPs with ultrafine particle size is achieved by the mineralization of Ftn subunits with Pt ions. Twenty four Ftn subunits spontaneously form a larger structure upon addition of Pt ions as confirmed by DLS analysis which shows a shift in hydrodynamic diameter from ~9.5 to ~13.3 nm (Figure 3a). TEM characterization of negatively stained (Pt)Ftn shows a cage-like ferritin shell surrounding a dark core (Figure 3b). The size of the core−shell structure of ~13 nm is in excellent agreement with that obtained by DLS analysis. After chemical reduction of Pt ions, the HRTEM image in Figure 3c shows clearly that the dark core of Pt NPs is about 2−3 nm in diameter, indicating that the ferritin core is not fully occupied by the Pt ions. The lattice fringe measured is ~0.23 nm, which conforms to plane (111) of the face-centered-cubic crystallographic structure of Pt. Quantification of Pt content by ICP-AES shows that ~20 Pt atoms are encapsulated per 24-meric ferritin. It should be mentioned that the addition of a lower molar ratio of K_2PtCl_4 (e.g., 10 Pt atoms/24-mer ferritin) can also induce the ferritin shell formation with no obvious size change of the Pt NPs observed. In contrast, if a higher molar ratio of K_2PtCl_4 (e.g., 100 Pt/24-mer ferritin) was added, the ferritin would be salted out and form precipitates instantly. Following the reduction step, (Pt)Ftn was subsequently deposited on the graphene surface through a self-assembly process. The deposition of the hydrophilic Ftn-coated Pt NPs onto the hydrophobic graphene is probably facilitated by the presence of hydrophobic patches on the ferritin shell. Following the deposition of the (Pt)Ftn, the ferritin shell is removed by thermal treatment. TEM characterization in Figure 4 and

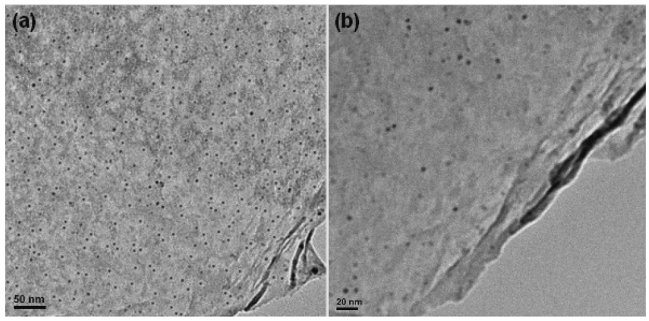

Figure 4. TEM images of a Pt/3D-graphene composite by immobilization of 5 mL of (Pt)Ftn (a) and 1 mL of (Pt)Ftn (b); the (Pt)Ftn concentration was 1.0 mM.

Figure S2 (Supporting Information (SI)) shows that the immobilized Pt NPs with a size of ~3 nm are still monodispersed on the graphene surface. This result suggests that the ferritin shell effectively prevents the aggregation of the ultrafine Pt NPs during the thermal treatment, and the removal of the ferritin shell has no obvious effect on the shape and size of Pt NPs. Prior to TEM characterization, the Pt/graphene was subjected to 20 min ultrasonic treatment. The Pt NPs were observed to remain attached, suggesting that the Pt NPs adhere stably on the graphene surface. The composition and crystal structure of the Pt/graphene were further characterized by EDX (Figure S3, SI) and XRD (Figure S4, SI) analysis, respectively. The three diffraction peaks located at 40.0°, 46.2°, and 67.5° can be ascribed to the (111), (200), and (220) diffraction of face-centered-cubic Pt. The peak at ~26° indicates the graphitic nature of 3D-graphene. It is worth mentioning that the amount of the immobilized Pt NPs on graphene can be adjusted to some extent by changing the amount of (Pt)Ftn added. For example, if the amount of (Pt)Ftn added was reduced to 20% of the standard loading

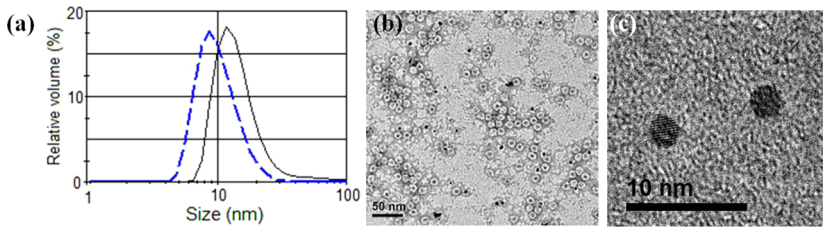

Figure 3. DLS measurement of the hydrodynamic diameters of ferritin before (dashed) and after (solid) the addition of Pt ions (a); TEM image of (Pt)Ftn stained with 1% uranyl acetate (b); and HRTEM image of the (Pt)Ftn without stain (c).

dx.doi.org/10.1021/am3022366 | ACS Appl. Mater. Interfaces 2013, 5, 782−787

amount, less Pt NPs were loaded. The more sparse distribution of the Pt NPs is observed under an electron microscope (Figure 4b).

Electrochemical Measurement. The high conductivity of the graphene network modified with ultrafine Pt NPs has been proposed as an electrocatalyst in fuel cells. Figure 5a shows the

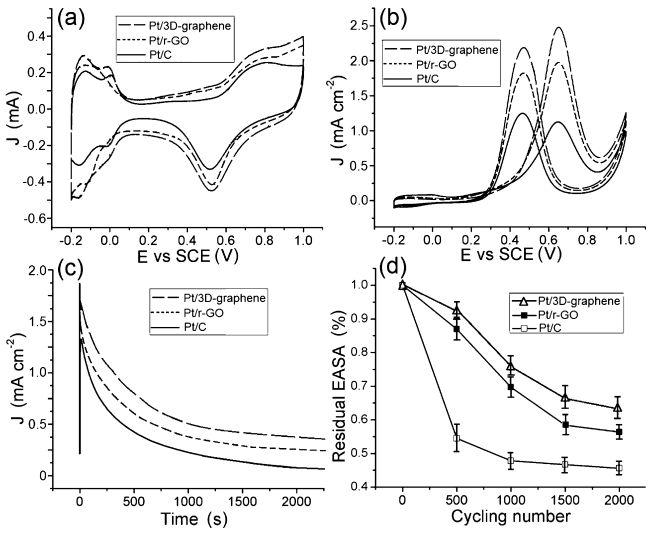

Figure 5. CVs of Pt/3D graphene, Pt/r-GO, and Pt/C electrodes in 0.5 M H_2SO_4 solution (a) and in 0.5 M H_2SO_4 + 1.0 M methanol solution; scan rate: 50 mV s^{-1} (b); current−time curves of Pt/3D graphene, Pt/r-GO, and Pt/C electrodes in 0.5 M H_2SO_4 + 1.0 M methanol solution at +0.5 V (c); residual EASAs of the three electrodes after continuous CV cycling from −0.2 to 1.0 V in 0.5 M H_2SO_4 solution (d).

cyclic voltammetry curves (CVs) of the Pt/3D graphene and commercial Pt/C catalyst in 0.5 M H_2SO_4 solution. To further highlight the advantage of the 3D graphene, the chemically reduced GO decorated with Pt NPs (Pt/r-GO) has also been included for comparison, and the Pt mass ratio of the two Pt/graphene composites are adjusted to that of Pt/C (20 wt %). Similar Pt electrochemical CV behaviors have been observed for all three electrodes with hydrogen underpotential adsorption/stripping in the potential range of −0.2 to 0.05 V, the double-layer capacitance region from 0.1 to 0.3 V, and metal oxidation/reduction peaks in the range of 0.4−0.9 V. The higher double-layer capacitance of the two graphene-based electrodes compared to that of the commercial Pt/C indicates that graphene support has a larger surface area than the C support. The observation is in good agreement with the Brunauer−Emmett−Teller (BET) N_2 adsorption−desorption result which shows that the specific surface areas of the 3D graphene and carbon black (VulcanXC-72) are ∼670 and ∼250 m^2 g^{-1}, respectively. The integrated hydrogen adsorption area shows that the electrochemically active surface area (EASA) of Pt for Pt/3D graphene is ∼30% higher (16.8 m^2 g^{-1}) than for Pt/C (13.1 m^2 g^{-1}). The larger EASA of Pt in the Pt/3D graphene should be ascribed to better dispersion of the ultrafine Pt NPs (2−3 nm) on 3D graphene. A similarly higher EASA of Pt has also been observed on Pt/r-GO, suggesting that the Pt NPs are more accessible on the r-GO compared to Pt/C at similar deposition of 20 wt %. The distinct structures may contribute to the EASA difference between the Pt/3D graphene and Pt/rGO. Pt/3D graphene is a free-standing interconnected electrode, while Pt/r-GO is dispersed powder which is immobilized on the glassy carbon electrode with the help of Nafion.

Figure 5b shows the CVs of the three electrocatalysts in 0.5 M H_2SO_4 + 1 M methanol solution. The anodic peak in the forward scan located at ∼0.70 V is attributed to the direct oxidation of methanol adsorbed on the catalyst surface,[38] and the peak at ∼0.5 V during the backward scan is ascribed to the oxidation of intermediate carbonaceous residues formed on the catalyst during the forward scan.[38,39] There still exists much controversy with regard to the origin of the oxidation peak in the backward scan. The reverse anodic current peak has been proposed to originate from the direct methanol oxidation on the reduced Pt surface.[40] Thus, the oxidation peak during the forward scan is usually used to evaluate the catalytic activity of the electrocatalyst. The specific current density at ∼0.7 V on Pt/3D graphene is higher than that on Pt/r-GO and over twice as high compared to that of Pt/C. The integrated EASA in the reported current densities suggests that the observed enhancement should originate from the intrinsic high catalytic activity of the Pt/3D graphene which is the result of its unique structure. The ratio of two anodic current densities, I_f/I_b, has been used to describe catalyst susceptibility to poisoning, provided that the reverse anodic peak originates from the oxidation of intermediate carbonaceous residues formed on the catalyst during the forward scan.[41,42] For commercial Pt/C, the I_f/I_b value is 0.77, while for Pt/r-GO and Pt/3D-graphene, this value is 1.05 and 1.13, respectively, indicating that the oxidation of methanol on the Pt/3D graphene is more efficient during the forward scan.

The long-term catalytic activities of the three electrocatalysts are also evaluated by recording their steady-state current responses with time. Figure 5c presents the chronoamperometry data under 0.5 V in a solution containing 0.5 M H_2SO_4 and 1.0 M CH_3OH for 2250 s. The fast initial current decay for all three catalysts should be due to the formation of double-layer capacitance. The subsequent slow decay may be due to the adsorption of a small amount of CO_{ads} species on catalyst surfaces during methanol electrooxidation.[43] The cause of current decay has also been proposed to stem from the adsorption of SO_4^{2-} on catalyst surfaces inhibiting the reaction active sites.[44] The current gradually reached a quasi-equilibrium steady state in long-term operation. The steady-state current on the Pt/3D graphene is higher than those on Pt/r-GO and Pt/C and is in good agreement with the CV study results. Both CV and the steady-state current response indicate that the Pt/3D graphene composite has a higher catalytic performance.

The stability of the Pt/3D graphene composite is also significantly enhanced compared with those of both Pt/r-GO and Pt/C. To examine the electrochemical stability of Pt/3D graphene, continuous CV cycling was perfromed from −0.2 to 1.0 V in 0.5 M H_2SO_4 solution at room temperature. The EASAs of the Pt/3D graphene and Pt/r-GO nanocomposites decrease slowly with increasing scan cycles and retain ∼65% and ∼57% of the initial value, respectively, after 2000 cycles (Figure 5d). In contrast, under the same conditions the EASA of Pt/C drops to ∼45% of its initial value.

The enhanced catalytic performance of the Pt/3D graphene compared with both Pt/r-GO and Pt/C should be attributed to its structure-related advantages such as exceptionally large void volume, high electrical conductivity, and high corrosion resistance. First, the interconnected pores may potentially offer low resistance to fluid flow and ensure efficient mass transfer during electrocatalysis. Second, the high electrical

dx.doi.org/10.1021/am3022366 | ACS Appl. Mater. Interfaces 2013, 5, 782−787

conductivity is essential for efficient electron conduction through the electrode. Compared to the powder form (r-GO), the unique monolithic nature can maintain its conductivity better by eliminating junction resistance when used as an electrode. Third, high corrosion resistance of the graphene material can significantly reduce the support corrosion problem which has been identified as one of the main reasons for the fuel cell's rapid performance loss.[45]

To further demonstrate the advantage of the present Pt/3D graphene, we compared it with another Pt/3D graphene prepared by the pulse potential deposition process.[46] The electrochemical pulse deposition results in well-dispersed Pt NPs with size ranging from ∼10 to 30 nm on graphene, which is advantageous for MOR compared with Pt/3D graphene with Pt NP size of ∼100−200 nm prepared by conventional electrodeposition. Interestingly, the peak current density (forward scan) on the present Pt/3D graphene is ∼2.5 mA cm^{-2}, which is 50% higher compared to the Pt/3D graphene obtained by pulse electrodeposition for MOR under the same conditions (∼1.6 mA cm^{-2}).[46] Since the current densities have been normalized to the EASA of Pt, this enhancement can be safely ascribed to the monodispersed ultrafine Pt NPs formed by the templating strategy. The higher electrocatalytic activity of Pt NPs with a smaller size may be caused by a more strained Pt surface.

CONCLUSIONS

A Pt NPs/3D-graphene composite with Pt NP size of ∼3 nm has been successfully fabricated through ferritin-templated Pt NP systhesis and deposition on the graphene surface. The ferritin nanocage provides both high precision size control and facile self-assembly on the hydrophobic graphene surface by leveraging on the hydrophobic patches on its surface. An electrochemical test demonstrates that the Pt/3D graphene exhibits much enhanced electrocatalytic performance toward methanol oxidation compared with both Pt/r-GO and commercial Pt/C catalysts. The enhancement is demonstrated to be due to the structural advantage of the monodispersed ultrafine Pt NPs and the 3D graphene with interconnected conductive network. The present study suggests that the combination of graphene with the ferritin template is promising for the fabrication of novel electrocatalysts in fuel cells. Since the precise size control offered by the ferritin template is also very powerful for the synthesis of other functional NPs such as alloys, metal oxides, and QDs, this method should be suitable for the fabrication of other functional nanocomposites for wider applications.

ASSOCIATED CONTENT

Supporting Information

HRTEM, EDX, and XRD results of the Pt/graphene. This material is available free of charge via the Internet at http://pubs.acs.org.

AUTHOR INFORMATION

Corresponding Author

*E-mail: slim@ntu.edu.sg.

Present Address

⊥Tohoku University, Sendai 980-8577, Japan.

Author Contributions

‖Equal contribution to this work.

Notes

The authors declare no competing financial interest.

ACKNOWLEDGMENTS

We acknowledge the financial support from the NTU Institute of Nanosystems Interface Sciences and Technology (INSIST), AcRF Tier 2 grant from Ministry of Education of Singapore (MOE2011-T2-2-010), NNSF of China (21275076, 61076067), the Key Project of Chinese Ministry of Education (212058), Research Fund for the Doctoral Program of Higher Education of China (20123223110008), the National Basic Research Program of China (2012CB933300), Jiangsu Province Science Foundation for Six Great Talent Peak (RLD201103); and Xuewan Wang for technical assistance.

REFERENCES

(1) Lee, C.; Wei, X. D.; Kysar, J. W.; Hone, J. *Science* **2008**, *321*, 385.
(2) Novoselov, K. S.; Geim, A. K.; Morozov, S. V.; Jiang, D.; Zhang, Y.; Dubonos, S. V.; Grigorieva, I. V.; Firsov, A. A. *Science* **2004**, *306*, 666.
(3) Guo, S.; Sun, S. *J. Am. Chem. Soc.* **2012**, *134*, 2492.
(4) Guo, S.; Wen, D.; Zhai, Y.; Dong, S.; Wang, E. *ACS Nano* **2010**, *4*, 3959.
(5) Zhang, S.; Shao, Y.; Liao, H.; Engelhard, M. H.; Yin, G.; Lin, Y. *ACS Nano* **2011**, *5*, 1785.
(6) Li, Y. M.; Tang, L. H.; Li, J. H. *Electrochem. Commun.* **2009**, *11*, 846.
(7) Qiu, J.-D.; Wang, G.-C.; Liang, R.-P.; Xia, X.-H.; Yu, H.-W. *J. Phys. Chem. C* **2011**, *115*, 15639.
(8) Kou, R.; Shao, Y.; Mei, D.; Nie, Z.; Wang, D.; Wang, C.; Viswanathan, V. V.; Park, S.; Aksay, I. A.; Lin, Y.; Wang, Y.; Liu, J. *J. Am. Chem. Soc.* **2011**, *133*, 2541.
(9) Si, Y.; Samulski, E. T. *Chem. Mater.* **2008**, *20*, 6792.
(10) Venkateswara Rao, C.; Cabrera, C. R.; Ishikawa, Y. *J. Phys. Chem. C* **2011**, *115*, 21963.
(11) Xu, C.; Wang, X.; Zhu, J. *J. Phys. Chem. C* **2008**, *112*, 19841.
(12) Che, J. F.; Shen, L. Y.; Xiao, Y. H. *J. Mater. Chem.* **2010**, *20*, 1722.
(13) Dong, X. C.; Wang, X. W.; Wang, L. H.; Song, H.; Zhang, H.; Huang, W.; Chen, P. *ACS Appl. Mater. Interfaces* **2012**, *4*, 3129.
(14) Shang, N. G.; Papakonstantinou, P.; Wang, P.; Ravi, S.; Silva, P. *J. Phys. Chem. C* **2010**, *114*, 15837.
(15) Jasuja, K.; Linn, J.; Melton, S.; Berry, V. *J. Phys. Chem. Lett.* **2010**, *1*, 1853.
(16) Wang, H. L.; Casalongue, H. S.; Liang, Y. Y.; Dai, H. J. *J. Am. Chem. Soc.* **2010**, *132*, 7472.
(17) Liu, Y.; Dong, X.; Chen, P. *Chem. Soc. Rev.* **2012**, *41*, 2283.
(18) Kim, J.-W.; Lillehei, P. T.; Park, C. *J. Mater. Chem.* **2012**, *22*, 8408.
(19) Dong, X. C.; Su, C. Y.; Zhang, W. J.; Zhao, J. W.; Ling, Q. D.; Huang, W.; Chen, P.; Li, L. J. *Phys. Chem. Chem. Phys.* **2010**, *12*, 2164.
(20) Chen, Z. P.; Ren, W. C.; Gao, L. B.; Liu, B. L.; Pei, S. F.; Cheng, H. M. *Nat. Mater.* **2011**, *10*, 424.
(21) Liu, J.; Fu, S.; Yuan, B.; Li, Y.; Deng, Z. *J. Am. Chem. Soc.* **2010**, *132*, 7279.
(22) Ueno, T.; Suzuki, M.; Goto, T.; Matsumoto, T.; Nagayama, K.; Watanabe, Y. *Angew. Chem., Int. Ed.* **2004**, *43*, 2527.
(23) Zhang, Y.; Tang, Z.; Wang, J.; Wu, H.; Lin, C.-T.; Lin, Y. *J. Mater. Chem.* **2011**, *21*, 17468.
(24) Uchida, M.; Klem, M. T.; Allen, M.; Suci, P.; Flenniken, M.; Gillitzer, E.; Varpness, Z.; Liepold, L. O.; Young, M.; Douglas, T. *Adv. Mater.* **2007**, *19*, 1025.
(25) Sana, B.; Johnson, E.; Sheah, K.; Poh, C. L.; Lim, S. *Biointerphases* **2010**, *5*, Fa48.
(26) Fan, J.; Yin, J. J.; Ning, B.; Wu, X. C.; Hu, Y.; Ferrari, M.; Anderson, G. J.; Wei, J. Y.; Zhao, Y. L.; Nie, G. J. *Biomaterials* **2011**, *32*, 1611.

(27) Liu, G. D.; Wu, H.; Wang, J.; Lin, Y. H. *Small* **2006**, *2*, 1139.
(28) Sana, B.; Poh, C. L.; Lim, S. *Chem. Commun.* **2012**, 48.
(29) Dong, X. C.; Li, B.; Wei, A.; Cao, X. H.; Chan-Park, M. B.; Zhang, H.; Li, L. J.; Huang, W.; Chen, P. *Carbon* **2011**, *49*, 2944.
(30) Dong, X. C.; Wang, P.; Fang, W. J.; Su, C. Y.; Chen, Y. H.; Li, L. J.; Huang, W.; Chen, P. *Carbon* **2011**, *49*, 3672.
(31) Johnson, E.; Cascio, D.; Sawaya, M. R.; Gingery, M.; Schroder, I. *Structure* **2005**, *13*, 637.
(32) Hosein, H. A.; Strongin, D. R.; Allen, M.; Douglas, T. *Langmuir* **2004**, *20*, 10283.
(33) Hummers, W. S.; Offeman, R. E. *J. Am. Chem. Soc.* **1958**, *80*, 1339.
(34) Ferrari, A. C.; Meyer, J. C.; Scardaci, V.; Casiraghi, C.; Lazzeri, M.; Mauri, F.; Piscanec, S.; Jiang, D.; Novoselov, K. S.; Roth, S.; Geim, A. K. *Phys. Rev. Lett.* **2006**, *97*, 187401.
(35) Graf, D.; Molitor, F.; Ensslin, K.; Stampfer, C.; Jungen, A.; Hierold, C.; Wirtz, L. *Nano Lett.* **2007**, *7*, 238.
(36) Huang, Y. X.; Dong, X. C.; Shi, Y. M.; Li, C. M.; Li, L. J.; Chen, P. *Nanoscale* **2010**, *2*, 1485.
(37) Dresselhaus, M. S.; Jorio, A.; Hofmann, M.; Dresselhaus, G.; Saito, R. *Nano Lett.* **2010**, *10*, 751.
(38) Sun, Z. P.; Zhang, X. G.; Liang, Y. Y.; Li, H. L. *J. Power Sources* **2009**, *191*, 366.
(39) Ureta-Zanartu, M. S.; Alarcon, A.; Munoz, G.; Gutierrez, C. *Electrochim. Acta* **2007**, *52*, 7857.
(40) He, Q. G.; Chen, W.; Mukerjee, S.; Chen, S. W.; Laufek, F. *J. Power Sources* **2009**, *187*, 298.
(41) Deivaraj, T. C.; Lee, J. Y. *J. Power Sources* **2005**, *142*, 43.
(42) Musthafa, O. T. M.; Sampath, S. *Chem. Commun.* **2008**, 67.
(43) Kabbabi, A.; Faure, R.; Durand, R.; Beden, B.; Hahn, F.; Leger, J. M.; Lamy, C. *J. Electroanal. Chem.* **1998**, *444*, 41.
(44) Guo, J. W.; Zhao, T. S.; Prabhuram, J.; Chen, R.; Wong, C. W. *Electrochim. Acta* **2005**, *51*, 754.
(45) Wang, X.; Li, W. Z.; Chen, Z. W.; Waje, M.; Yan, Y. S. *J. Power Sources* **2006**, *158*, 154.
(46) Maiyalagan, T.; Dong, X.; Chen, P.; Wang, X. *J. Mater. Chem.* **2012**, *22*, 5286.